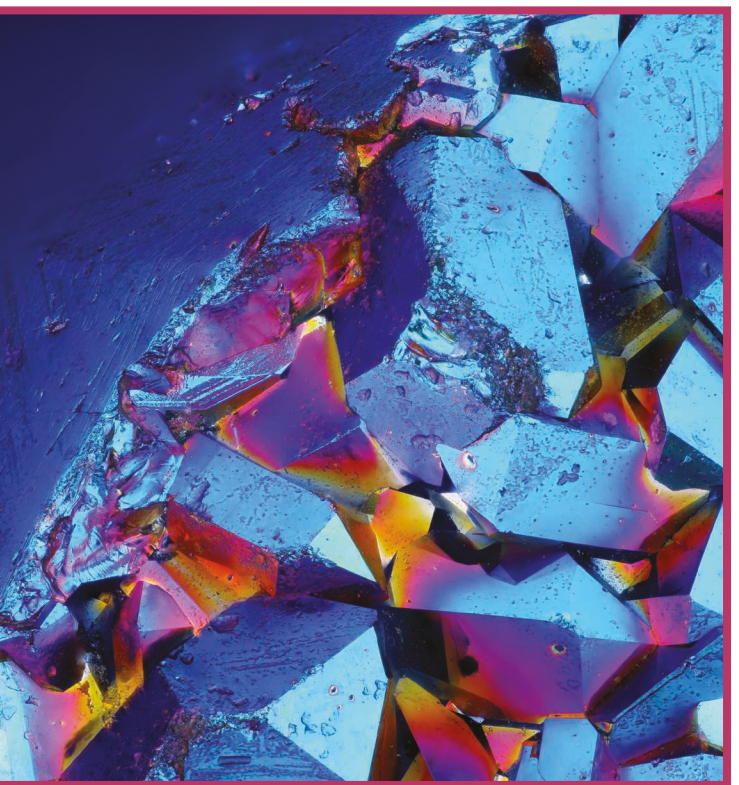
S.V. Venkatakrishnan, K. Aditya Mohan, Amir Koushyar Ziabari, and Charles A. Bouman

# Algorithm-Driven Advances for Scientific CT Instruments

From model-based to deep learning-based approaches



©SHUTTERSTOCK.COM/TOMATIT

ultiscale 3D characterization is widely used by materials scientists to further their understanding of the relationships between microscopic structure and macroscopic function. Scientific computed tomography (SCT) instruments are one of the most popular choices for 3D nondestructive characterization of materials at length scales ranging from the angstrom scale to the micron scale. These instruments typically have a source of radiation (such as electrons, X-rays, or neutrons) that interacts with the sample to be studied and a detector assembly to capture the result of this interaction (see Figure 1). A collection of such high-resolution measurements is made by reorienting the sample, which is mounted on a specially designed stage/holder after which reconstruction algorithms are used to produce the final 3D volume of interest. The specific choice of which instrument to use depends on the desired resolution and properties of the materials being imaged. The end goal of SCT scans includes determining the morphology, chemical composition, or dynamic behavior of materials when subjected to external stimuli. In summary, SCT instruments are powerful tools that enable 3D characterization across multiple length scales and play a critical role in furthering the understanding of the structure–function relationships of different materials.

## **Challenges in SCT**

The archetypal form of CT involves illuminating a sample with a beam, measuring a projection image corresponding to the transmitted or scattered signal, and collecting a set of measurements by rotating the sample (or the source–detector system) about a single axis in the 0–180° or 0–360° range followed by a reconstruction routine that inherently assumes a linear relationship between the measured signal (or some preprocessed version) and the quantity to be reconstructed. While these types of systems are common in medical X-ray CT, there are several aspects that make the SCT problem different and challenging. These challenges can be grouped into a few broad categories.

## Limited-angle measurements

In applications such as electron tomography (one of the most popular methods for angstrom-scale and nanoscale

Digital Object Identifier 10.1109/MSP.2021.3123594 Date of current version: 28 December 2021 3D imaging), the mechanical limitations of the sample holder along with the unique shape of the samples may only allow for acquiring data in a limited angular range  $(+/-60^{\circ})$  [1], as illustrated in Figure 2(a). Limited-angle data sets can also occur in other SCT modalities when the sample hold-

ers are designed for specialized tasks. An example of this type of holder is the diamond anvil cell [2] (used for studying the properties of materials under extremely high pressure), which strongly attenuates the incident beam in certain orientations [see Figure 2(b)]. In summary, driven by the

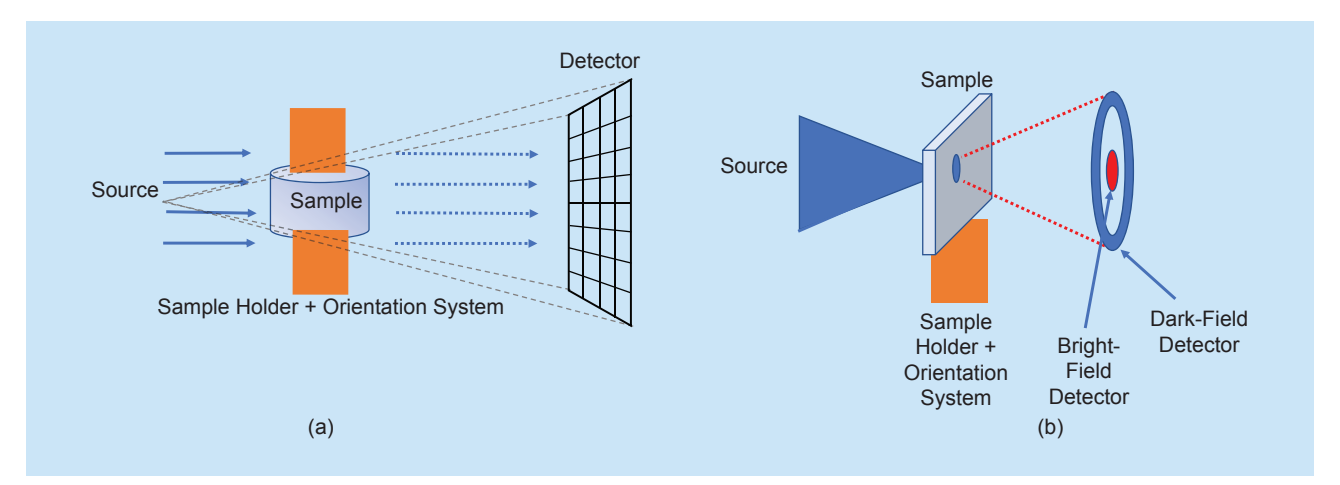


FIGURE 1. A schematic of common acquisition setups used in SCT systems. (a) The setup used in parallel-beam and cone-beam X-ray/neutron CT systems. (b) The setup used in electron/X-ray microscope-based scanning probe systems. In each case a source is used to illuminate the sample of interest, and a detector system (an area detector, a point detector, or an annular detector) captures the result of this interaction. The sample, which is mounted on a holder, is reoriented to make a collection of measurements. The archetypal acquisition geometry for SCT instruments is to rotate the sample about a single axis perpendicular to the direction of the incident source and make a collection of measurements followed by reconstruction using analytic algorithms.

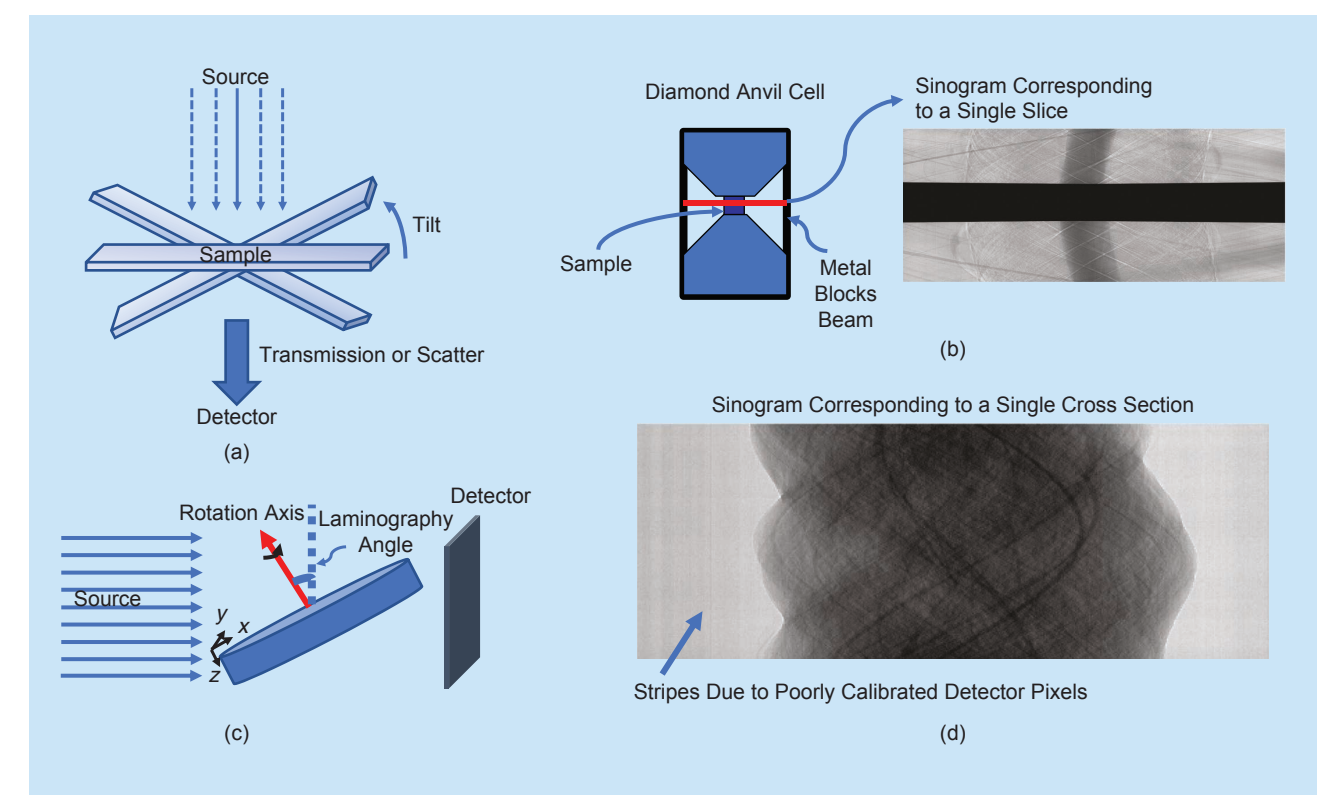


FIGURE 2. Some of the challenges in SCT. Because of (a) and (b) the mechanical limitations of the sample holder, (c) the shape of the sample being imaged, and (d) poorly calibrated detectors, it can be challenging to obtain accurate 3D reconstructions from the resulting limited-view, sparse, low signal-to-noise ratio (SNR) data. Note that a *sinogram* refers to a particular organization of the measured data from a CT scan, where the vertical axis corresponds to the orientation, and the horizontal axis corresponds to a single row of the detector.

flexibility required to engineer sample holders to perform novel experiments, limited-angle data sets can occur in important SCT applications, making it challenging to obtain high-quality reconstructions.

# Unconventional measurement geometries

The acquisition geometry used in SCT instruments can be different compared to that of the conventional single-axis CT setup. The need for new geometries is driven by the requirement to measure samples with unique shapes, which may not yield sufficient signal-to-noise ratio (SNR) data in certain orientations. For example, a technique called laminography has been developed to measure samples that are lamellar, such as integrated circuit boards. In laminography [3] the sample is tilted and rotated about this new tilt axis to measure a signal of sufficient strength on the detector [Figure 2(c)]. Unlike the case of a conventional single-axis CT, analytic reconstruction algorithms for novel geometries are not readily available, thereby impeding the use of novel acquisition schemes. In summary, the unique shapes of various samples to be scanned dictate a greater degree of flexibility in the measurement geometries for SCT instruments and require novel reconstruction algorithms.

# Sparse, low SNR, and poorly calibrated data

SCT instruments are typically purchased from commercial vendors or built at scientific user facilities (SUFs), where a source of radiation/particles (e.g., a high flux of neutrons from a nuclear reactor or monochromatic X-rays from a synchrotron) forms the basis for a unique imaging capability. In both situations, SCT instruments are often very expensive and are treated as a shared resource, leading to a need for making the fewest possible measurements to extract the relevant scientific information from the study. As a result, reducing the number of measurements (sparse view data) and the duration of each measurement (leading to low SNR) can be critical to maximize the throughput to make SCT instruments available to a large number of users. Sparse-view and low-SNR data can also occur in the SCT experiments where the sample can suffer radiation damage as with the case of biomaterials. These types of data are also common in high-speed time-resolved 4D-CT experiments [4], where the goal is to image how a sample is changing at the microscopic scale when subjected to external stimuli.

SCT measurements can also be corrupted by different signals that are independent of the sample. For example, it is common in conventional X-ray micro-CT [5] and neutron-CT [3] systems to have spurious radiation strike the detector, leading to a high-amplitude signal in a few measurements. Furthermore, the detectors used in SCT instruments may not be perfectly calibrated. One common example of this phenomenon is the observation of correlated "streaks" in the measured sinograms (a way of organizing the CT data so that the data corresponding to all orientations for a single slice can be easily visualized) because the gain associated with each detector pixel is different [see Figure 2(d)]. These imperfections in the

data due to outliers and poorly calibrated detectors result in reconstructions with streak and ring artifacts when a conventional reconstruction algorithm is directly applied to the data. In summary, it is challenging to achieve a higher throughput, reduce damage to samples by lowering their exposure to source radiation, and improve the spatiotemporal resolution of 4D CT while preserving image fidelity because of the sparse, low-SNR, and poorly calibrated measurements.

## Large data sets

SCT scans are usually conducted to obtain 3D information at high resolutions. With the advent of faster, higher-pixel-resolution detectors and the need to measure larger samples, there has been an explosion in the size of SCT data sets. For example, it is common across SCT applications to use detectors that are approximately  $2,000 \times 2,000$  pixels and for the corresponding CT reconstructions to have sizes of the order of  $2,000 \times 2,000 \times 2,000$  voxels. In the case of hyperspectral SCT instruments [6], [7], the sizes of the data sets are even larger depending on the number of hyperspectral channels. For 4D CT, this problem is compounded since the number of measurements increases linearly with time. In summary, it can be challenging to obtain high-quality reconstructions in reasonable time frames for SCT applications.

# Conventional approaches to SCT

Despite the significant advances made in developing various hardware components of SCT instruments (source, lenses, sample holders, detectors, and so on), until recently, there has been less focus on the development of reconstruction algorithms to deal with the various challenges encountered. A common practice has involved measuring a large amount of data corresponding to the Nyquist criterion [8] or the maximum number of measurements at a reasonable SNR that can be made in an allocated amount of time in the case of a shared instrument at SUFs. Following the acquisition, the measurements are preprocessed (using, e.g., filters to suppress outliers, heuristic correction of miscalibrated data, and normalization) and reconstructed using analytic algorithms, such as filtered backprojection (FBP) [8], gridrec [9], or Feldkamp-Davis-Kreiss [10] because of their widespread availability and low computational complexity. However, the performance of these algorithms can be poor when dealing with nonlinearities in the measurement, the presence of high levels of noise, and the limited number of measurements—which are common in the context of SCT applications, as discussed in the section "Challenges in Scientific CT." The reliance on the use of analytic reconstruction techniques, in turn, limits the characterization capability of SCT instruments by resulting in significant artifacts from sparse-view, limited, and low-SNR data sets. Additionally, the reliance on analytic reconstruction algorithms has led to an inefficient usage of the instruments by requiring the collection of large amounts of data to ensure the reconstructed images are of high quality.

In the rest of this article, we will present an overview of recent advances in nonlinear reconstruction algorithms that have enabled significant improvements in the performance of SCT instruments—enabling faster, more accurate, novel imaging capabilities. We emphasize that, while this article focuses on SCT applications where a linear forward model accurately describes the physics of image formation (up to pointwise normalization), there are important CT applications, such as phase-contrast imaging and ptychography, where the underlying physics-based model is significantly more complicated, but for which the ideas presented here are equally relevant.

We will first focus on model-based image reconstruction (MBIR) algorithms [11] that formulate the inversion as solving a high-dimensional optimization problem involving a datafidelity term (which includes a physics-based forward model) and a regularization term (based on a model for the sample to be imaged). By accurately modeling the physics and noise statistics of the measurement and combining it with state-ofthe art regularizers, we will highlight how dramatic improvements are being made in the performance of several types of SCT instruments. While the development of MBIR methods has demonstrated that it is possible to dramatically improve the performance of CT instruments, these techniques are computationally expensive for the high-resolution scans encountered in SCT applications. This bottleneck had led researchers to adapt and develop noniterative deep learning (NIDL) approaches based on convolutional neural networks [12] to attain similar improvements to those of the MBIR methods in certain scenarios. In the last part of the article, we will present an overview of recent approaches using DL-based algorithms for improving SCT instruments. We will summarize different approaches developed to address the tomographic inversion including data-domain and image-domain learning. The recent advances have shown that DL-based methods are a promising tool to complement MBIR methods because of their rapid inference time on large high-resolution SCT data sets while enabling similar improvements in image quality, and reduction of the scan time.

### **MBIR for SCT instruments**

MBIR [11] refers to an umbrella term for joint maximum a posteriori (MAP) estimation [13] or a regularized inversion approach to solving image reconstruction problems. In the MBIR framework, the reconstruction task is formulated as

$$(\hat{x}, \hat{\psi}) \leftarrow \underset{x \in \Omega, \psi \in \Psi}{\operatorname{argmin}} \{ l(y; x, \psi) + r(x; \beta) \}, \tag{1}$$

where y is a vector containing the measurements, x is a vector corresponding to the object to be reconstructed, l is a data-fidelity function that enforces consistency of the reconstruction with the measured data based on a physics-based forward model,  $\psi$  is a vector of calibration parameters associated with the measurement,  $\Omega$  and  $\Psi$  are constraint sets, and r is a regularization term with parameters  $\beta$ . In the context of MAP estimation [11], l corresponds to the negative log-likelihood function, and r corresponds to the negative log-prior function. MBIR approaches have been used for several imaging problems and have enabled significant dose reduction in

medical X-ray CT and accelerations of magnetic resonance imaging scans while preserving image quality compared to conventional approaches in the respective fields. The main challenges in the design of MBIR methods are the formulation of the cost function of the type in (1) by an appropriate choice of the physics-based forward model, noise-dependent data-fidelity loss, l, application-dependent regularizer, r, and the design of fast optimization algorithms to obtain a minimum of the cost function. In what follows, we will present the ways in which different MBIR algorithms have been developed for 3D and 4D SCT.

# Volumetric CT

The goal of volumetric CT is to reconstruct some property of a sample, such as the linear attenuation coefficient, scatter coefficient, or complex-valued index of refraction, in three dimensions. The most straightforward adoption of MBIR for SCT has been for conventional transmission or scatter-type CT, using a data-fidelity term of the form

$$l(y; x) = \frac{1}{2} \|y - Ax\|_{W}^{2}, \tag{2}$$

where *W* is a diagonal matrix containing the inverse noise variance in the measurements, *A* is the tomographic projection operator, and *y* either contains the log-normalized transmission measurements [14] or the measured signal itself [15] from each orientation. This model can be derived by assuming that the measurements are corrupted by additive white Gaussian noise or by using a quadratic approximation to the log-likelihood function based on Poisson statistics [16]. A variety of regularizers has been combined with the model in (2), but one popular class is the generalized Markov random field-based (MRF) regularizer [16], which includes the popular anisotropic total variation and the q-generalized Gaussian MRF [17]. These regularizers are of the form

$$r(x; \beta_s) = \beta_s \sum_{\{i,j\} \in \chi} w_{ij} \rho(x_i - x_j), \tag{3}$$

where  $\rho$  is a function that penalizes differences between neighboring voxels,  $\beta_s$  is a parameter that adjusts the weight assigned to the regularization terms,  $\chi$  is a set containing all pairs of neighboring voxels in three dimensions, and  $w_{ij}$  are weights associated with each pair of voxels. MBIR algorithms based on combining the models in (2) and (3) have been developed for parallel-beam electron tomography [14], [15], [18], [19], synchrotron-based X-ray CT [2], [5], and neutron tomography [20], enabling significantly higher-quality reconstructions compared to the analytic reconstruction algorithms from the sparse, limited-view, and low-SNR data routinely encountered in these applications.

The development of MBIR methods has shown that it is possible to achieve a similar image quality as that of the analytic reconstruction methods using about one-half or even one-fourth the typical number of measurements made [2], [20] at X-ray and neutron-CT instruments. This potentially enables two to four times more samples to be measured at these instruments than would have been possible when analytic

reconstruction methods were used. Another advantage of using the model in (2) is that the W matrix can be used as a simple means to adjust the relative weight of each measurement to reject subsets of measurements that are corrupted. Prior to the development of MBIR methods, the standard practice in several SCT applications has been to leave out entire projection data sets corresponding to a specific orientation because of the corruption of a subset of the data, resulting in an inefficient use of the measurements. For example, in [2], the effective use of the weight matrix helped suppress streak artifacts due to beam blocking caused by the strong attenuation from a diamond anvil cell sample holder [see Figure 2(b)] in a CT study about the behavior of materials under extremely high pressure. Finally, we note that while the quadratic data-fidelity term in (2) has been demonstrated to be useful across several SCT applications, alternate models derived by assuming the measurements have a Poisson distribution of the form

$$l(y; x) = \sum_{i=1}^{M} \{ [Ax]_i - y_i \log([Ax]_i) \},$$
 (4)

where M is the total number of measurements, have also been used along with regularizers of the form in (3) for low-dose SCT applications [6].

The MBIR approach using the models in (2) and (3) has also been developed for novel CT geometries. One such example is for *laminography*, where the sample is rotated about a tilted axis instead of the conventional perpendicular axis [see Figure 2(c)] to image samples that might otherwise heavily attenuate the beam and thereby require a very long scan time. The authors in [3] have developed an MBIR technique based on a new forward model term that incorporates the new acquisition geometry into the *A* matrix in (2). In addition to the benefits of enabling high-quality reconstructions from sparse-view and low-SNR data, MBIR approaches are useful for such novel geometries because

analytic reconstruction algorithms may not be readily available or can result in significant artifacts in the reconstructed images.

Similar MBIR approaches have also been recently developed for single-particle cryoelectron microscopy [21], a widely used angstrom-scale 3D bioimaging technique in which the reconstruction involves inverting ultralow-dose data from parallel-beam projection images corresponding to arbitrary orientations of the sample defined by a set of Euler angles. This line of research has demonstrated that it is possible to obtain high-quality 3D reconstructions by using MBIR techniques despite the complicated geometry of acquisition associated with the SCT instrument, thereby allowing scientists to be able to have an additional control variable for their experimental acquisition.

Another powerful advantage of using MBIR methods for SCT is the ability to account for unknown calibration parameters associated with the measurement. In cases where the measurements are impacted by poorly calibrated detectors, conventional algorithms can produce reconstructions with significant artifacts. To address poorly calibrated data, the authors in [5] and [15] modified the forward model in (2) to account for parameters such as detector gains and offsets. For example, in dark-field electron tomography [15], the gains and offsets of the detector are typically not measured. To address this challenge, a forward model of the form

$$l(y; x, I, d) = \frac{1}{2} \|y - IAx - d\|_{W}^{2}$$
 (5)

was proposed, where I is a diagonal matrix containing the unknown gain associated with the detected signal at each projection orientation, and d is a vector containing the unknown offsets. Using this model along with constraints on I resulted in an algorithm that significantly improved the image quality compared to the traditional FBP method that was widely used in the field (see Figure 3). A similar approach [5] was

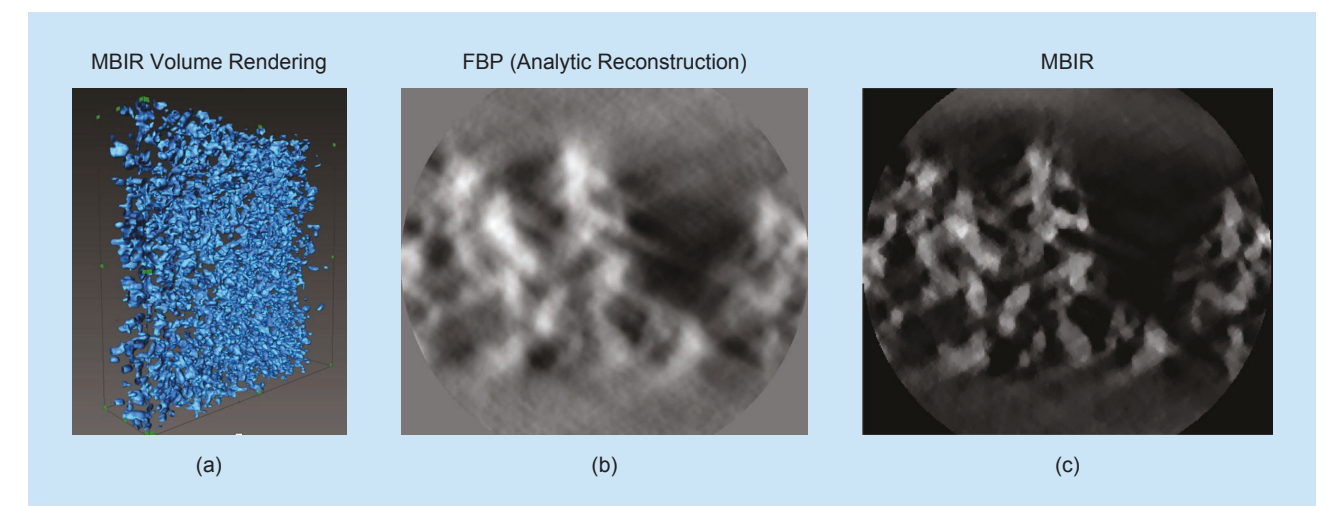


FIGURE 3. A comparison of MBIR with FBP on an experimental high-angle annular dark-field electron tomography data set of titanium dioxide nanoparticles. The illustration includes (a) a 3D MBIR volume rendering and a single cross section from a 3D reconstruction obtained using the (b) FBP and the (c) MBIR approach. The data set contained 60 projection images of size 1,024 × 1,024 pixels measured in an angular range of ± 60°. In spite of the low SNR, sparse, limited-view data with unknown calibration parameters, the MBIR method significantly suppresses artifacts compared to the FBP method. This highlights how the use of powerful reconstruction algorithms can improve the imaging capability of SCT instruments. (Source: [15]; adapted with permission.)

used to address the challenge of poorly calibrated detectors, where each pixel in the detector has a different gain [as shown in Figure 2(d)], by modeling the unknown detector gains into the MBIR framework, leading to reconstructions that significantly suppress the ring artifacts that commonly result from such miscalibrations (see Figure 4).

Finally, new forward models have also been formulated to address the challenge of outliers due to gamma/X-ray/neutron strikes and spurious scatter due to Bragg diffraction when imaging samples that contain single-crystal domains. Because it is complicated to explicitly develop a physics-based model for such data, researchers have used new data-fidelity terms based on heavy-tailed distributions for the *l* in (1) including the generalized Huber function [5], [14] and the Student *t* function [22] (see Figure 5) in the MBIR framework. Specifically, new forward models of the form

$$l(y; x) = \frac{1}{2} \Gamma((y - Ax)\sqrt{W}), \tag{6}$$

where  $\Gamma: \mathbb{R}^M \to \mathbb{R}$ ,  $\Gamma(e) = \sum_{i=1}^M \gamma(e_i)$ , and  $\gamma$  is of the form shown in Figure 5, have been used in [5], [14], and [22]. While it is more complicated to find a minimum of the

# (a) MBIR

**FIGURE 4.** A single (cropped) cross section from a 3D reconstructed volume of a carbon fiber data set acquired using a synchrotron X-ray instrument. (a) Because of miscalibrated detectors, direct use of the analytic algorithm results in a reconstruction with ring artifacts. (b) However, the use of a specially designed MBIR method suppresses the ring artifacts while preserving detail and reducing noise. (Source: [5]; adapted with permission.)

resulting cost function, such an algorithm can further improve image quality compared to baseline MBIR algorithms based on quadratic data-fidelity and analytic reconstruction algorithms.

# Time-resolved CT

SCT is also used to image the temporal dynamics of an object that is undergoing change in response to external stimuli, such as varying temperature and pressure. This mode of imaging, commonly known as *4D CT*, is used to image the evolution of samples in three dimensions with respect to time. In materials science, 4D CT is used to study dynamic phenomena, such as solidification, phase transformations, crack formation, and battery degradation. 4D CT is performed using a variety of radiation sources that include X-rays, electrons, and neutrons, at resolutions ranging from nanometer-to micron-length scales mostly using the setup of the type in Figure 1(a).

One way in which 4D CT has been performed is by subjecting the material to the desired stimuli (like a certain pressure), acquiring a conventional CT for that specific stimulus point and repeating the process for different stimuli. The measurements corresponding to each CT scan are then reconstructed into a single 3D volume of the 4D reconstruction. Indeed, the 3D MBIR methods of the section "Volumetric CT" can be directly applied to these scenarios to reduce the time required to collect the data for a single reconstruction. However, if the goal of the study is to perform in situ imaging of the dynamics of rapidly changing material properties, then the overall problem becomes significantly more challenging.

Figure 6 illustrates a data-acquisition scheme for 4D CT of a sample that is changing continuously in the course of the measurement. To conduct in situ 4D CT, the sample is rotated continuously about a single axis, and the projection data

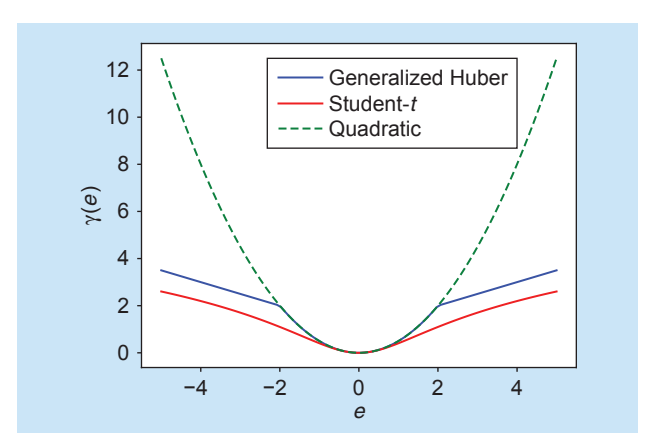


**FIGURE 5.** Penalty functions used for robust MBIR. In several SCT applications, the measurements can be corrupted by outliers due to strong diffraction from crystalline samples, and gamma-ray/X-ray/neutron strikes on the detector in addition to detector noise. By using penalty functions based on heavy-tailed probability density functions, such as the generalized Huber function or the Student *t* function instead of the conventional quadratic function (dotted line) for the data-fidelity term, it is possible to obtain high-quality reconstructions with minimal pre/postprocessing.

are measured using a low-exposure setting on the detector to reduce motion blur. Each measurement corresponds to the projection of the sample at a certain time and orientation with respect to the incident beam. Obtaining a 3D reconstruction corresponding to each time point is not possible because we only have a single projection image corresponding to that state of the sample. Therefore, algorithms designed for 4D CT of continuously varying samples have used different strategies to acquire and process the data. The most common approach is to group the data corresponding to a few orientations (see Figure 6) and perform a 3D-CT reconstruction for each set with the implicit assumption that the sample does not change in the time window corresponding to each set. However, because of the widespread use of analytic reconstruction algorithms, there has been a tendency to believe that each set needs to contain measurements that cover a full angular range (typically 180°) and that a large number of such measurements (of the order of a few thousand for typical detectors) is required to obtain highfidelity reconstructions.

While some of these challenges can be overcome in specific situations (for example, the imaging of samples that are exhibiting a periodic motion [23]), the overall use of analytic reconstruction approaches has limited the application of 4D CT to the imaging of relatively slow processes. To address the challenge of obtaining high-fidelity in situ 4D CT, researchers have adapted the MBIR methods discussed in the section "Volumetric CT" combined with synergistic changes in the way the data are acquired [25]. One prominent approach is the time-interlaced MBIR (TIMBIR) [4] method, in which the data are acquired such that the orientation angles ( $\theta_i$  in Figure 6)

corresponding to each set are sparsely spaced over an angular range of  $180^{\circ}$  and interlaced with the angles in the other sets. This interlacing offers increased measurement diversity compared to a standard accelerated/sparse-view system in which the collection of  $\theta_i$  in each set is the same. Using a forward model that is similar to (6) for the data-fidelity term in (1), the authors proposed a regularizer of the form

$$r(x; \beta_{s}, \beta_{t}) = \beta_{s} \sum_{l=1}^{L} \sum_{\{i, j\} \in \chi_{s}} w_{ij} \rho_{s}(x_{l,i} - x_{l,j}) + \beta_{t} \sum_{i} \sum_{\{m, n\} \in \chi_{t}} w_{mn} \rho_{t}(x_{m,i} - x_{n,i}),$$
 (7)

where  $\beta_s$  and  $\beta_t$  are the regularization parameters for spatial and temporal regularization, respectively,  $x_t$  corresponds to the 3D reconstruction for set l,  $\chi_s$  and  $\chi_t$  represent the sets for the pairs of voxel neighbors across space and time, respectively, and  $w_{ij}$  and  $w_{mn}$ , are weights associated with voxel pairs, which are set to be inversely proportional to the distance/time between the neighbors. Using the TIMBIR algorithm, it has been demonstrated (see Figure 7) that it is possible to obtain high-fidelity 4D reconstructions while accelerating the scan by a factor of 32 compared to what would have been possible if the traditional protocol were used [4].

The use of regularizers that exploit local spatiotemporal correlations to improve reconstruction fidelity [similar to (7)] has been widely studied in the research literature. While the regularizer (7) that exploits local spatiotemporal correlations is useful, researchers have also developed more sophisticated regularizers based on deformation fields or motion models [26],

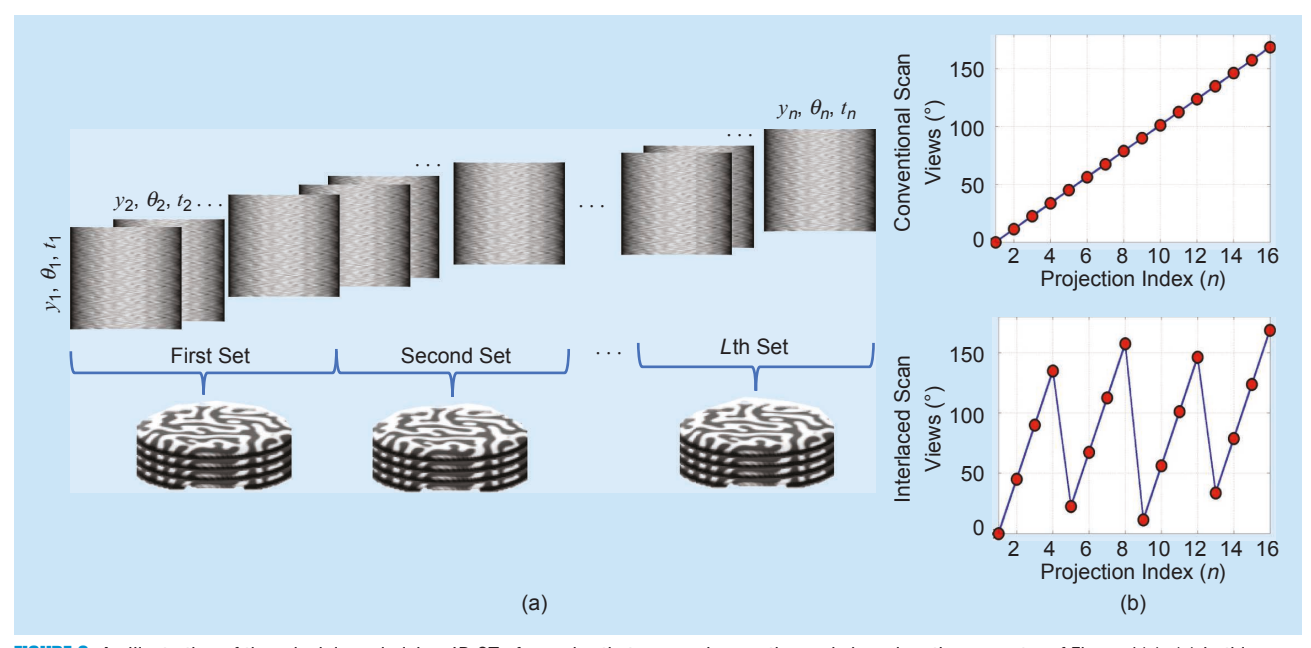


**FIGURE 6.** An illustration of the principle underlying 4D CT of samples that are varying continuously based on the geometry of Figure 1(a). (a) In this case, each measured projection image  $(y_i)$  corresponds to a specific orientation  $(\theta_i)$  and duration of time depending on the exposure and frame rate of the detector. (b) The projections can be acquired by gradually orienting the sample in a 180° range or by using an interlaced scan, as shown in the plots. In theory, each projection corresponds to a different state of the underlying 3D object. However, in practice, reconstruction algorithms are designed by assuming small variations, grouping collections of projection images, and obtaining a 3D reconstruction corresponding to each collection.

demonstrating that it is possible to further improve the quality of the MBIR approaches for 4D CT. Other approaches that enforce spatiotemporal sparsity by relying on the similarity between nonlocal image patches have also been explored. In summary, the key advantage of using MBIR approaches is that the measured data can be grouped in several different ways (each set potentially corresponding to sparse, low-SNR, and limited-view sets) and jointly used for reconstruction, thereby enabling high-fidelity images at unprecedented temporal resolutions.

# Accelerating MBIR for large data sets

While methods to accelerate MBIR depend on the specifics of the forward model, much of the recent research is focused on conventional parallel-beam CT using models of the form (2) and (3) because of its widespread use across SCT applications. Broadly, the solutions to the MBIR cost function based on (2) and (3) for conventional CT can be categorized into parallel update methods (like gradient descent) and sequential update methods (like coordinate descent [16]). In either case, such algorithms are computationally expensive since they involve a large number of forward projection (multiplication by A) and backprojection (multiplication  $A^{t}$ ) operations, which are typical in any iterative solution to the cost-function minimization. For 4D CT, this problem is compounded since the number of views can be an order of magnitude larger than for 3D CT. The computational complexity of the forward and backward projection operations also increases with the size of the reconstructed volumes. Thus, it becomes difficult to obtain real-time feedback on the success of an experiment because of the long computational times of MBIR algorithms. Furthermore, tuning of the regularization and other free parameters becomes tedious in the absence of fast reconstructions. Thus, it is important to speed up MBIR algorithms to increase their adoption for SCT.

One popular approach to speed up MBIR is to use novel optimization techniques that hasten algorithmic convergence. The techniques to improve algorithmic convergence are typically dependent on the choice of the optimization algorithm

used for reconstruction. Multiresolution approaches use reconstruction at coarser resolution scales to initialize reconstruction at a finer resolution. Such approaches are typically used to improve the convergence of iterative coordinate descent (ICD) algorithms since ICD has poor low-frequency convergence [4], [15]. Another approach to speed up MBIR is to use high-performance compute (HPC) clusters for distributed parallel computing [27]-[29]. This approach relies on modifications to existing optimization algorithms that enable distributed computation on supercomputing HPC clusters. In [4], an approach to distributed parallel 4D CT is presented in which several 2D slices of each 3D volume over multiple time frames are reconstructed in parallel. However, this particular strategy of parallelizing over several 2D slices provides limited speedup improvements since the reconstruction of each slice is computationally expensive. Recently, algorithmic approaches for parallel reconstruction of voxels within each slice have also been proposed. These large-scale parallelization approaches have led to a dramatic acceleration of reconstruction times of large volumes by distributing the computation across thousands of cores—enabling reconstructions of size  $2,160 \times 2,560 \times 2,560$  in about 24 s using 146,880 cores of an HPC cluster [27].

# Regularization parameters for MBIR

The eventual goal of SCT scans is either to discover new features of scientific relevance (like the appearance of a crack from a material under stress) or to perform a measurement (such as the porosity of a manufactured part) from the reconstructed volumes. The choice of regularization function and the associated parameters have a significant impact on the quality (noise and resolution) of reconstructions obtained using the MBIR approach. Therefore, algorithms to automatically choose the regularization parameters that produce images that maximize the performance of the end goal will be impactful. However, because of the diversity of measurement scenarios, samples scanned, and resolution values, the task of automatically choosing regularization parameters even for

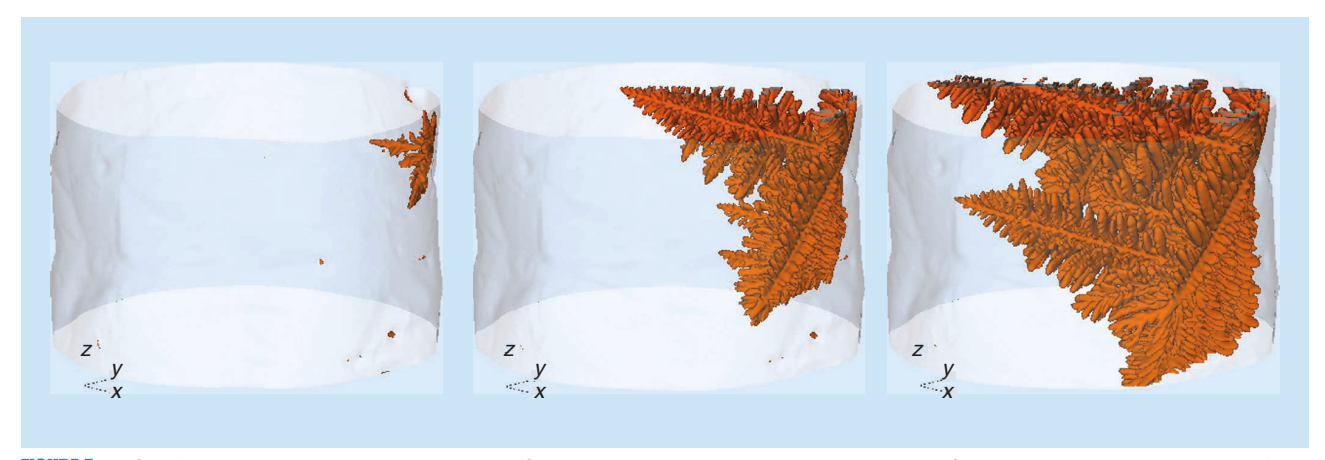


**FIGURE 1.** 4D CT of growing dendrites in a slowly cooled Al–Cu alloy measured using synchrotron-based X-ray CT using the TIMBIR method [24]. A few reconstructed volumes from the 4D reconstruction that contain 3D frames every 1.8 s at a voxel resolution of approximately 1 µm, showing that it is possible to obtain high spatiotemporal resolution using MBIR approaches.

a fixed choice of regularization function of the form in (3) is challenging. Furthermore, the regularization parameters are often dimensionless quantities that do not have a straightforward interpretation for end users of SCT instruments, making them complicated to set in an intuitive manner.

While some general approaches for setting the regularization parameters in the context of model-based reconstruction have been proposed ([30] and references therein), they have not been widely adapted for SCT. These approaches can be broadly categorized as methods that require evaluation of multiple reconstructions (L-curve, generalized cross validation, and so on), those that set the value based on "balancing" the data-fidelity and regularization terms, and Bayesian methods that jointly estimate the regularization parameter and reconstructions. The previous approaches are not guaranteed to produce reconstructions of the best quality matched to the task for which SCT is being carried out. The extensions of these methods for applications like 4D CT and hyperspectral CT have also not been explored. Current adaptations of MBIR for SCT have mainly relied on an empirical choice of parameters to attain some desirable visual image quality (a certain level of noise, sharpness of edges, and so on). Typically, the parameters are varied; a few slices from the 3D volume are reconstructed to manage the computational complexity, and for each choice of parameters the reconstruction is evaluated, sometimes based on a predefined metric [31]. In summary, the regularization parameters for SCT applications have largely been set in an empirical manner, making the automated choice of these parameters an important future research direction.

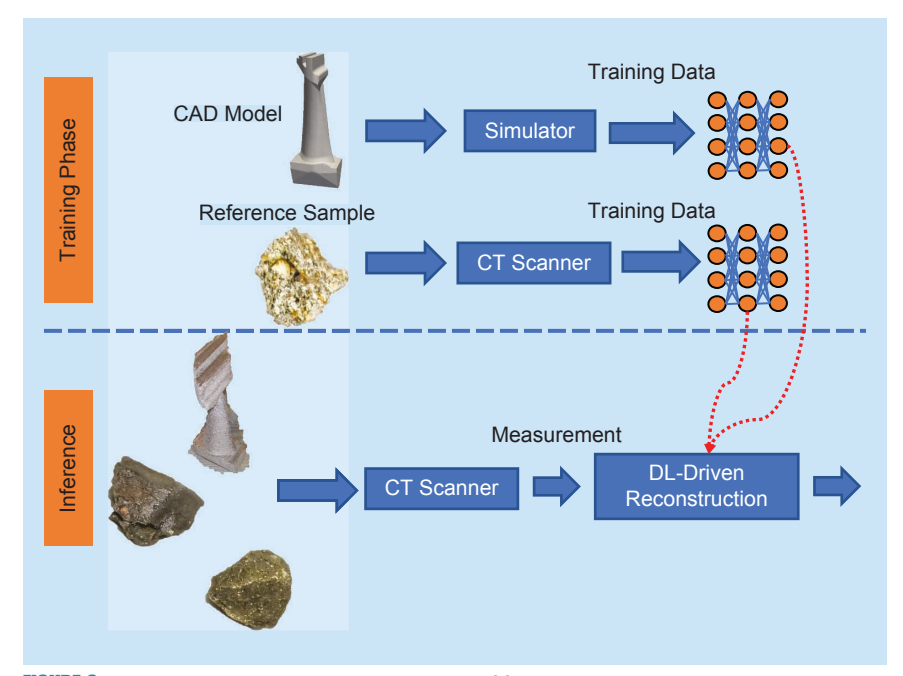


**FIGURE 8.** Illustration of approaches used for DL-based SCT. The training data are either generated from a reference scan of a representative sample or from a CAD-based model when appropriate. Because of the diversity of samples to be measured using SCT, it is challenging to train a single general-purpose neural network that works across a wide variety of samples; hence, current research has focused on training neural networks for a specific collection of samples.

# Deep learning (DL)-based CT reconstruction

DL-based algorithms have recently been developed to address several challenges that occur in the context of CT reconstruction [32]. These algorithms can be broadly categorized into iterative and noniterative approaches [12]. Iterative approaches to DL are based on explicitly deriving the iterative updates that result from solutions to the MBIR formulations of the section "Volumetric CT" and then replacing certain blocks with trainable deep neural networks (DNNs) to obtain high-quality reconstructions. By contrast, noniterative approaches are based on training a DNN to learn to preprocess the measurements followed by the use of a conventional analytic reconstruction algorithm. Alternately, noniterative deep learning (NIDL)-based algorithms can be applied in the reconstruction domain by designing a DNN to learn to suppress common artifacts that occur when using analytic reconstruction algorithms. In the context of SCT, NIDL-based approaches have garnered significant interest because of their low computational complexity at inference time and simple portability to GPUs that can enable fast reconstructions for the large data sets from SCT instruments.

While NIDL-based reconstruction has been widely explored in the context of applications such as medical X-ray CT, there are several challenges in adapting these methods for SCT applications. First, SCT instruments are used to scan a wide variety of samples; therefore, the training data for DNNs must be chosen carefully. From an algorithm designer's perspective, it may be impossible to obtain sufficient data to train a single generic DNN that can be applied for any sample that has to be imaged under different measurement scenarios (geometry, number of views, SNR, and so on). Furthermore, obtaining high-quality

reference data sets to train neural networks can be time consuming/expensive; therefore, in SCT applications we might only be able to make a very small number of reference measurements. Finally, the central problems associated with SCT are high dimensional, involving 3D spatial and 4D spatiotemporal reconstructions. This leaves open the question of how to effectively adapt popular DNN architectures that are designed for 2D imaging applications, such as the U-Net [33] and DnCNN [34], to the multidimensional case.

Supervised NIDL algorithms have been developed for SCT, mainly in the context of scanning collections of similar samples, 4D CT, or those situations for which a 3D model is available, as shown in Figure 8. If the goal of an experiment is to accelerate the measurement of a large collection of similar samples (a set of rocks, additively manufactured parts, and so on), then one or more of the

samples can be scanned in a manner such that we can obtain training data for a DNN that is designed to obtain high-quality reconstruction from sparse/limited-view/low-SNR data. A variety of different approaches to obtain training data, choice of network architecture, and loss functions have been explored in the context of developing NIDL for SCT. For example, in [36] an NIDL approach was developed to obtain high-quality reconstruction from low-dose X-ray CT data. A few pairs of low-dose and high-dose projection images were measured, followed by the use of an encoder-decoder-based DNN trained using a Wasserstein and perceptual loss function to map between the low-dose and high-dose projection data. Since the data are extremely limited, the acquired images were split into smaller patches and data-augmentation techniques were used to stably train the DNN, which has a very large number of parameters. The trained network was then used to obtain highquality CT reconstruction by processing new low-dose measurements using the DNN followed by the use of an analytic reconstruction approach—both steps can be performed rapidly for the large data sets encountered in this application. Another NIDL approach for SCT has involved measuring a complete low-dose and regular-dose CT scan from a reference sample and reconstructing them using an analytic reconstruction algorithm. These data are used to train a DNN to map between the low-dose and high-dose 3D reconstruction. One challenge in such approaches is that there may only be a single 3D volume

pair to train the network. To address this limited-data challenge, methods of splitting the 3D volume into smaller patches combined with data-augmentation methods, such as flipping and rotation, are used to increase the size of the training set [37], [38].

In contrast to this approach, a new neural network architecture-mixedscale densenet (MS-DNet)—was proposed in [35], [39], which has an order-of-magnitude fewer parameters than other popular DNN architectures [33], [34] and a large-receptive field, making it a strong candidate for the limited training data encountered in SCT applications. Furthermore, to exploit the 3D structure of the data, instead of training a fully 3D DNN, the works in [35], [37], and [39] have used a 2.5D strategy [40], where the input to the neural network is a collection of adjacent slices (modeled as channels), and the target output is a single image. The overall approach of using NIDL based on making one high-quality volumetric reference has demonstrated that it is possible to accelerate acquisition and yet obtain high-quality 3D reconstructions from extremely sparse-view data (see

Figure 9), which can be used to dramatically improve the throughput of SCT instruments at shared facilities [41]. However, the generalization ability of different approaches, which drives the need for measuring new training data sets, remains an open question.

NIDL-based algorithms are also being used when a CAD of a part to be scanned is available (typical in the case of additively manufactured objects) [38]. The goal of these studies is to reduce the measurement time for high-resolution CT and to obtain high-quality reconstructions from samples that can potentially introduce nonlinearities, such as beam hardening, into the measurement. For example, in [38] a framework was developed to generate training data for DNNs by simulating X-ray CT scans of a specific part in a polyenergetic X-ray micro-CT system. To obtain realistic data, a simulator was developed that embeds various defects in the CAD model, accounts for complex phenomena, such as beam hardening of the incident X-rays, and generates the sparse, low-SNR data that occur during an experimental CT scan. Since the ground truth is known, a 2.5D DNN was trained based on a conventional mean-squared loss function to suppress the noise, streaks, and beam-hardening artifacts that are encountered when using analytic reconstruction approaches. Once this network was trained, it was applied to experimental data of samples corresponding to the CAD model, demonstrating promising preliminary results in obtaining higher-quality reconstructions from accelerated scans while enhancing the detectability of defects.

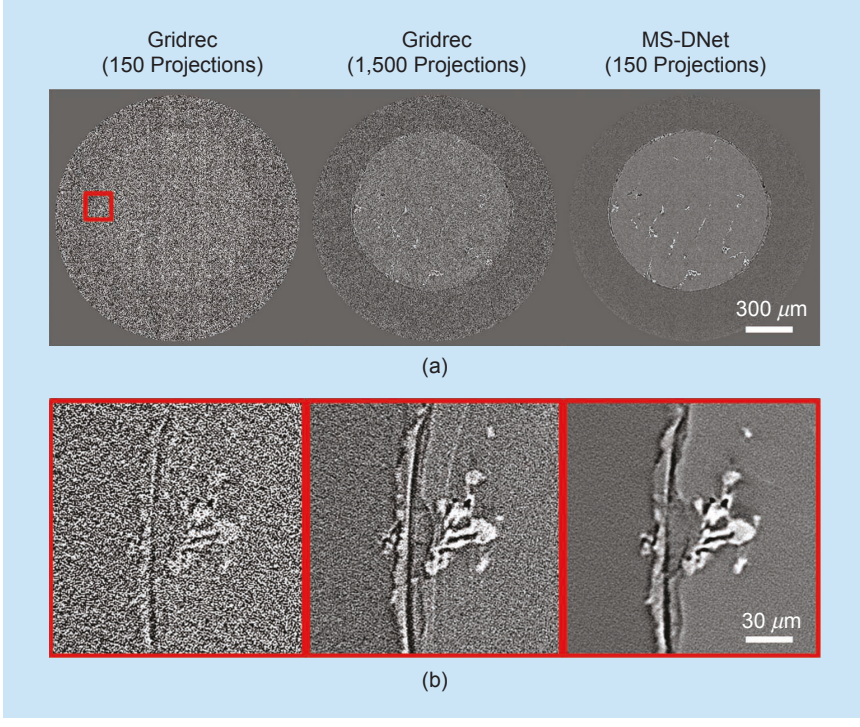


FIGURE 9. Illustration of the use of DL-based reconstruction for a sparse-view and low-SNR synchrotron X-ray CT data set of an aluminum sample. The figure shows a (a) single cross section from a 3D reconstruction using an analytic reconstruction algorithm (gridrec) and a DL-based reconstruction based on the MS-DNet including a (b) patch selected from the original cross section to better highlight the details. Notice that using one-tenth the number of measurements typically made, the DNN-based approach is able to produce a higher-quality reconstruction compared to the analytic reconstruction approach. (Source: [35].)

Finally, self-supervised DL approaches have also been used for enhancing the quality of SCT reconstructions, especially when obtaining pairs of matched training data for supervised learning is not possible. A recent example is [42], where a DNN was trained from a single low-SNR experimental CT scan by splitting the acquired data in an effective manner. Specifically, by obtaining a pair of 3D reconstructions from subsets of the measured data, a DNN based on the MS-DNet [35] was trained to map between pairs of these reconstructed slices. Once trained, the same network can be applied to the entire noisy measurement to produce a high-fidelity reconstruction. The method, deemed Noise2Inverse, was further expanded in [43] and successfully applied to 3D and 4D CT. A substantial reduction in acquisition time was achieved while reducing noise and maintaining image quality. This type of self-supervised learning approach can be particularly useful for SCT applications, such as neutron CT or lab-based X-ray CT, where obtaining high-resolution scans is extremely time consuming.

## **Conclusions**

In this article, we presented an overview of how advanced image reconstruction algorithms are enabling improvements in the performance of SCT instruments. These algorithmic advances are a powerful complement to the decades of advances in hardware technologies in being able to obtain high-fidelity images while enabling a dramatic acceleration of the time required to make measurements. While the research highlighted in this article has demonstrated the potential for algorithmdriven approaches for SCT instruments, there are still several open questions, including the choice of regularization function and parameters for MBIR methods, algorithmic- and computation-driven acceleration for larger data sets, and the further investigation of the choice of architecture, parameters and loss functions for DL-based reconstruction. A version of this article with an extended set of references is available at https://arxiv .org/abs/2104.08228.

# **Acknowledgments**

This manuscript has been authored by UT-Battelle, LLC, under contract DE-AC05-00OR22725 with the U.S. Department of Energy (DOE). The U.S. Government and the publisher, by accepting the article for publication, acknowledge that the U.S. Government retains a nonexclusive, paid-up, irrevocable, worldwide license to publish or reproduce the published form of this manuscript, or allow others to do so, for U.S. Government purposes. The U.S. DOE will provide public access to these results of federally sponsored research in accordance with the DOE Public Access Plan (http:// energy.gov/downloads/doe-public-access-plan). Part of this work was performed under the auspices of the U.S. DOE by Lawrence Livermore National Laboratory under contract DE-AC52-07NA27344 (release number LLNL-JRNL-821781). This work was partially supported by Oak Ridge National Laboratory via the Artificial Intelligence Initiative. S.V. Venkatakrishnan was partially supported by the U.S. DOE Office of Basic Energy Science. Amir Koushyar Ziabari was supported by the U.S. DOE, Office of Energy Efficiency and Renewable Energy, Advanced Manufacturing Office, under contract DE-AC05-00OR22725 with UT-Battelle, LLC. This work was partially supported by NSF grant number CCF-1763896.

## **Authors**

S.V. Venkatakrishnan (venkatakrisv@ornl.gov) received his Ph.D. degree from the School of Electrical and Computer Engineering at Purdue University in 2014. He is currently an R&D staff member in the Multimodal Sensor Analytics group at Oak Ridge National Laboratory, Oak Ridge, Tennessee, 37831, USA, developing computational imaging algorithms in support of the lab's efforts in ultrasound, X-ray, electron-, and neutron-based systems. His research interests include computational imaging, inverse problems, and machine learning. He is a Senior Member of IEEE, a member of the IEEE Computational Imaging Technical Committee, and an associate editor of IEEE Transactions on Computational Imaging (2018–present).

K. Aditya Mohan (mohan3@llnl.gov) received his Ph.D. degree in electrical and computer engineering from Purdue University in 2017. He is affiliated with the Computational Engineering Division at Lawrence Livermore National Laboratory, Livermore, California, 94551, USA. His research interests include computational imaging, inverse problems, and machine learning. As a principal investigator, he is also experienced in leading research projects in these areas. He is a Senior Member of IEEE.

Amir Koushyar Ziabari (ziabariak@ornl.gov) received his Ph.D. degree from the Department of Electrical and Computer Engineering (ECE) at Purdue University in 2016. He is an R&D staff scientist in the Multimodal Sensor Analytics group at Oak Ridge National Laboratory (ORNL), Oak Ridge, Tennessee, 37831, USA. Before joining ORNL, he was a postdoctoral student in the Integrated Imaging group in the Department of ECE at Purdue University. In his research on data science for science, he develops physics, signal processing, and machine/deep learning algorithms to process and analyze multiscale scientific imaging data. This includes his research on data analytic, data-driven, and physics-based image reconstruction and segmentation algorithms for advanced manufacturing (AM) to improve nondestructive evaluation and the state of the art in real-time monitoring of the AM process.

Charles A. Bouman (bouman@purdue.edu) received his Ph.D. in electrical engineering from Princeton University. He joined the faculty of the School of Electrical and Computer Engineering at Purdue University, West Lafayette, Indiana, 47907, USA, in 1989, where he is currently the Showalter Professor of Electrical and Computer Engineering and Biomedical Engineering. His research is in the area of computational imaging and sensing. He is a member of the National Academy of Inventors, a Fellow of IEEE, and a fellow of the American Institute for Medical and Biological Engineering, the Society for Imaging Science and Technology, and the International Society for Optics and Photonics. He was previously the editor-in-chief of IEEE Transactions on Image

*Processing*, a distinguished lecturer for the IEEE Signal Processing Society (SPS), and a vice president of Technical Activities for the SPS, during which time he led the creation of *IEEE Transactions on Computational Imaging*.

## References

- [1] P. Ercius, O. Alaidi, M. J. Rames, and G. Ren, "Electron tomography: A three-dimensional analytic tool for hard and soft materials research," *Adv. Mater.*, vol. 27, no. 38, pp. 5638–5663, 2015, doi: 10.1002/adma.201501015.
- [2] S. Venkatakrishnan, K. A. Mohan, K. Beattie, J. Correa, E. Dart, J. R. Deslippe, A. Hexemer, H. Krishnan et al., "Making advanced scientific algorithms and big scientific data management more accessible," *Electron. Imaging*, vol. 2016, no. 19, pp. 1–7, 2016, doi: 10.2352/ISSN.2470-1173.2016.19.COIMG-155.
- [3] S. Venkatakrishnan, E. Cakmak, H. Billheux, P. Bingham, and R. K. Archibald, "Model-based iterative reconstruction for neutron laminography," in *Proc. Signals, Syst. Comput.*, 2017, pp. 1864–1869.
- [4] K. Mohan, S. Venkatakrishnan, J. Gibbs, E. Gulsoy, X. Xiao, M. De Graef, P. Voorhees, and C. Bouman, "TIMBIR: A method for time-space reconstruction from interlaced views," *IEEE Trans. Comput. Imaging*, vol. 1, no. 2, pp. 96–111, June 2015, doi: 10.1109/TCI.2015.2431913.
- [5] K. A. Mohan, S. V. Venkatakrishnan, L. F. Drummy, J. Simmons, D. Y. Parkinson, and C. A. Bouman, "Model-based iterative reconstruction for synchrotron X-ray tomography," in *Proc. IEEE ICASSP*, 2014.
- [6] D. Gürsoy, T. Biçer, A. Lanzirotti, M. G. Newville, and F. D. Carlo, "Hyperspectral image reconstruction for X-ray fluorescence tomography," *Optics Express*, vol. 23, no. 7, pp. 9014–9023, 2015, doi: 10.1364/OE.23.009014.
- [7] S. Venkatakrishnan, Y. Zhang, L. Dessieux, C. Hoffmann, P. Bingham, and H. Bilheux, "Improved acquisition and reconstruction for wavelength-resolved neutron tomography," *J. Imaging*, vol. 7, no. 1, p. 10, 2021, doi: 10.3390/jimaging7010010.
- [8] A. C. Kak and M. Slaney, *Principles of Computerized Tomographic Imaging*. Philadephia, PA: Society for Industrial and Applied Mathematics, 2001.
- [9] F. Marone and M. Stampanoni, "Regridding reconstruction algorithm for real-time tomographic imaging," *J. Synchrotron Radiation*, vol. 19, no. 6, pp. 1029–1037, 2012, doi: 10.1107/S0909049512032864.
- [10] L. A. Feldkamp, L. C. Davis, and J. W. Kress, "Practical cone-beam algorithm," *JOSA A*, vol. 1, no. 6, pp. 612–619, 1984, doi: 10.1364/JOSAA.1.000612.
- [11] C. A. Bouman, "Model based image processing," 2013. [Online]. Available: https://engineering.purdue.edu/~bouman/publications/pdf/MBIP-book.pdf
- [12] M. T. McCann, K. H. Jin, and M. Unser, "Convolutional neural networks for inverse problems in imaging: A review," *IEEE Signal Process. Mag.*, vol. 34, no. 6, pp. 85–95, 2017, doi: 10.1109/MSP.2017.2739299.
- [13] A. Mohammad-Djafari, "Joint estimation of parameters and hyperparameters in a Bayesian approach of solving inverse problems," in *Proc. Int. Conf. Image Process.*, Sept. 1996, vol. 1, pp. 473–476.
- [14] S. Venkatakrishnan, L. Drummy, M. Jackson, M. De Graef, J. Simmons, and C. Bouman, "Model based iterative reconstruction for bright-field electron tomography," *IEEE Trans. Comput. Imaging*, vol. 1, no. 1, pp. 1–15, Mar. 2015, doi: 10.1109/TCI.2014.2371751.
- [15] S. Venkatakrishnan, L. Drummy, M. Jackson, M. De Graef, J. Simmons, and C. Bouman, "A model based iterative reconstruction algorithm for high angle annular dark field - scanning transmission electron microscope (HAADF-STEM) tomography," *IEEE Trans. Image Process.*, vol. 22, no. 11, pp. 4532–4544, Nov. 2013, doi: 10.1109/TIP.2013.2277784.
- [16] K. Sauer and C. Bouman, "Bayesian estimation of transmission tomograms using segmentation based optimization," *IEEE Trans. Nucl. Sci.*, vol. 39, no. 4, pp. 1144–1152, 1992, doi: 10.1109/23.159774.
- [17] J.-B. Thibault, K. Sauer, C. Bouman, and J. Hsieh, "A three-dimensional statistical approach to improved image quality for multislice helical CT," *Med. Phys.*, vol. 34, no. 11, pp. 4526–4544, 2007, doi: 10.1118/1.2789499.
- [18] Z. H. Levine, A. J. Kearsley, and J. G. Hagedorn, "Bayesian tomography for projections with an arbitrary transmission function with an application in electron microscopy," *J. Res. Nat. Inst. Standards Technol.*, vol. 111, no. 6, pp. 411–417, Nov. 2006, doi: 10.6028/jres.111.031.
- [19] Z. Saghi and P. A. Midgley, "Electron tomography in the (S)TEM: From nanoscale morphological analysis to 3D atomic imaging," *Annu. Rev. Mater. Res.*, vol. 42, no. 1, pp. 59–79, 2012, doi: 10.1146/annurev-matsci-070511-155019.
- [20] M. Abir, F. Islam, D. Wachs, and H.-K. Lee, "Sparse-view neutron CT reconstruction of irradiated fuel assembly using total variation minimization with poisson statistics," *J. Radioanalytical Nucl. Chem.*, vol. 307, no. 3, pp. 1967–1979, 2016, doi: 10.1007/s10967-015-4542-2.
- [21] L. Donati, M. Nilchian, C. O. S. Sorzano, and M. Unser, "Fast multiscale reconstruction for Cryo-EM," *J. Struct. Biol.*, vol. 204, no. 3, pp. 543–554, 2018, doi: 10.1016/j.jsb.2018.09.008.

- [22] D. Kazantsev, F. Bleichrodt, T. van Leeuwen, A. Kaestner, P. J. Withers, K. J. Batenburg, and P. D. Lee, "A novel tomographic reconstruction method based on the robust student's t function for suppressing data outliers," *IEEE Trans. Comput. Imaging*, vol. 3, no. 4, pp. 682–693, 2017, doi: 10.1109/TCI.2017.2694607.
- [23] S. M. Walker, D. A. Schwyn, R. Mokso, M. Wicklein, T. Müller, M. Doube, M. Stampanoni, H. G. Krapp et al., "In vivo time-resolved microtomography reveals the mechanics of the blowfly flight motor," *PLoS Biol.*, vol. 12, no. 3, p. e1001823, 2014, doi: 10.1371/journal.pbio.1001823.
- [24] J. W. Gibbs, K. A. Mohan, E. B. Gulsoy, A. J. Shahani, X. Xiao, C. A. Bouman, M. De Graef, and P. W. Voorhees, "The three-dimensional morphology of growing dendrites," *Sci. Rep.*, vol. 5, no. 1, p. 11824, 2015, doi: 10.1038/srep11824.
- [25] A. P. Kaestner, B. Munch, and P. Trtik, "Spatiotemporal computed tomography of dynamic processes," *Opt. Eng.*, vol. 50, no. 12, p. 123201, 2011.
- [26] G. Zang, R. Idoughi, R. Tao, G. Lubineau, P. Wonka, and W. Heidrich, "Space-time tomography for continuously deforming objects," vol. 37, no. 4, 2018, doi: 10.1145/3197517.3201298.
- [27] X. Wang, A. Sabne, P. Sakdhnagool, S. J. Kisner, C. A. Bouman, and S. P. Midkiff, "Massively parallel 3D image reconstruction," in *Proc. Int. Conf. High Performance Comput.*, *Netw.*, *Storage Anal.*, 2017, pp. 1–12.
- [28] T. Bicer, D. Gursoy, R. Kettimuthu, F. De Carlo, G. Agrawal, and I. T. Foster, "Rapid tomographic image reconstruction via large-scale parallelization," in *Euro-Par 2015: Parallel Processing*, J. L. Träff, S. Hunold, and F. Versaci, Eds. Berlin, Heidelberg: Springer Berlin Heidelberg, 2015, pp. 289–302.
- [29] X. Wang, A. Sabne, S. Kisner, A. Raghunathan, C. Bouman, and S. Midkiff, "High performance model based image reconstruction," in *Proc. 21st ACM SIGPLAN Symp. Principles Practice Parallel Programming (PPoPP '16)*, 2016, doi: 10.1145/2851141.2851163.
- [30] S. Ramani, T. Blu, and M. Unser, "Monte-Carlo SURE: A black-box optimization of regularization parameters for general denoising algorithms," *IEEE Trans. Image Process.*, vol. 17, no. 9, pp. 1540–1554, 2008, doi: 10.1109/TIP.2008.2001404.
- [31] S. Allner, A. Gustschin, A. Fehringer, P. B. Noël, and F. Pfeiffer, "Metric-guided regularisation parameter selection for statistical iterative reconstruction in computed tomography," *Sci. Rep.*, vol. 9, no. 1, pp. 1–10, 2019, doi: 10.1038/s41598-019-40837-7.
- [32] G. Wang, J. C. Ye, and B. De Man, "Deep learning for tomographic image reconstruction," *Nature Mach. Intell.*, vol. 2, no. 12, pp. 737–748, 2020, doi: 10.1038/s42256-020-00273-z.
- [33] O. Ronneberger, P. Fischer, and T. Brox, "U-net: Convolutional networks for biomedical image segmentation," in *Proc. Int. Conf. Medical Image Comput. Comput.-assisted Intervention*. Berlin: Springer-Verlag, 2015, pp. 234–241.
- [34] K. Zhang, W. Zuo, Y. Chen, D. Meng, and L. Zhang, "Beyond a gaussian denoiser: Residual learning of deep CNN for image denoising," *IEEE Trans. Image Process.*, vol. 26, no. 7, pp. 3142–3155, 2017, doi: 10.1109/TIP.2017.2662206.
- [35] D. M. Pelt, K. J. Batenburg, and J. A. Sethian, "Improving tomographic reconstruction from limited data using mixed-scale dense convolutional neural networks," *J. Imaging*, vol. 4, no. 11, pp. 128, 2018, doi: 10.3390/jimaging4110128.
- [36] X. Yang, V. De Andrade, W. Scullin, E. L. Dyer, N. Kasthuri, F. D. Carlo, and D. Gürsoy, "Low-dose X-ray tomography through a deep convolutional neural network," *Sci. Rep.*, vol. 8, no. 1, pp. 1–13, 2018, doi: 10.1038/s41598-018-19426-7.
- [37] Z. Liu, T. Bicer, R. Kettimuthu, D. Gursoy, F. D. Carlo, and I. Foster, "TomoGAN: Low-dose synchrotron X-ray tomography with generative adversarial networks: Discussion," *JOSA A*, vol. 37, no. 3, pp. 422–434, 2020, doi: 10.1364/JOSAA.375595.
- [38] A. Ziabari, S. Venkatakrishnan, M. Kirka, P. Brackman, R. Dehoff, P. Bingham, and V. Paquit, "Beam hardening artifact reduction in X-Ray CT reconstruction of 3D printed metal parts leveraging deep learning and CAD models," in *Proc. ASME Int. Mech. Eng. Congr. Expo.*, 2020, vol. 84492, p. V02BT02A043.
- [39] D. M. Pelt and J. A. Sethian, "A mixed-scale dense convolutional neural network for image analysis," *Proc. Nat. Acad. Sci.*, vol. 115, no. 2, pp. 254–259, 2018, doi: 10.1073/pnas.1715832114.
- [40] A. Ziabari, D. H. Ye, S. Srivastava, K. D. Sauer, J.-B. Thibault, and C. A. Bouman, "2.5D deep learning for CT image reconstruction using a multi-GPU implementation," in *Proc. 52nd Asilomar Conf. Signals, Syst. Comput.*, 2018, pp. 2044–2049, doi: 10.1109/ACSSC.2018.8645364.
- [41] S. V. Venkatakrishnan, A. Ziabari, J. Hinkle, A. W. Needham, J. M. Warren, and H. Z. Bilheux, "Convolutional neural network based non-iterative reconstruction for accelerating neutron tomography," *Mach. Learning: Sci. Technol.*, 2020.
- [42] A. A. Hendriksen, D. M. Pelt, and K. J. Batenburg, "Noise2inverse: Self-supervised deep convolutional denoising for tomography," *IEEE Trans. Comput. Imag.*, vol. 6, pp. 1320–1335, 2020, doi: 10.1109/TCI.2020.3019647.
- [43] A. A. Hendriksen, M. Bührer, L. Leone, M. Merlini, N. Vigano, D. M. Pelt, F. Marone, M. di Michiel et al., "Deep denoising for multi-dimensional synchrotron x-ray tomography without high-quality reference data," *Sci. Rep.*, vol. 11, no. 1, pp. 1–13, 2021, doi: 10.1038/s41598-021-91084-8.